CHAPTER IV

RESULTS AND DISCUSSION

4.1 Preliminary study of SFO crystallization of lysozyme

4.1.1 The solubility study by FBRM and SFO crystallizer testing

Figure 4.1 the solid dissolution in heating crystallizer until particle disappearance in FBRM monitor. Lysozyme showed the solubility through various temperatures versus amount of ammonium sulfate solution. In Figure 4.1 (a) solid lysozyme was added into crystallizer at −3 ˚C (0.4M) and the temperature gradually increased. The FBRM monitor showed high amount of solid in solution (Figure 4.1 (b)) and slowly decreased to base line with more clearly solution of lysozyme in crystallizer (Figure 4.1 (c)) at −1.5 ˚C.

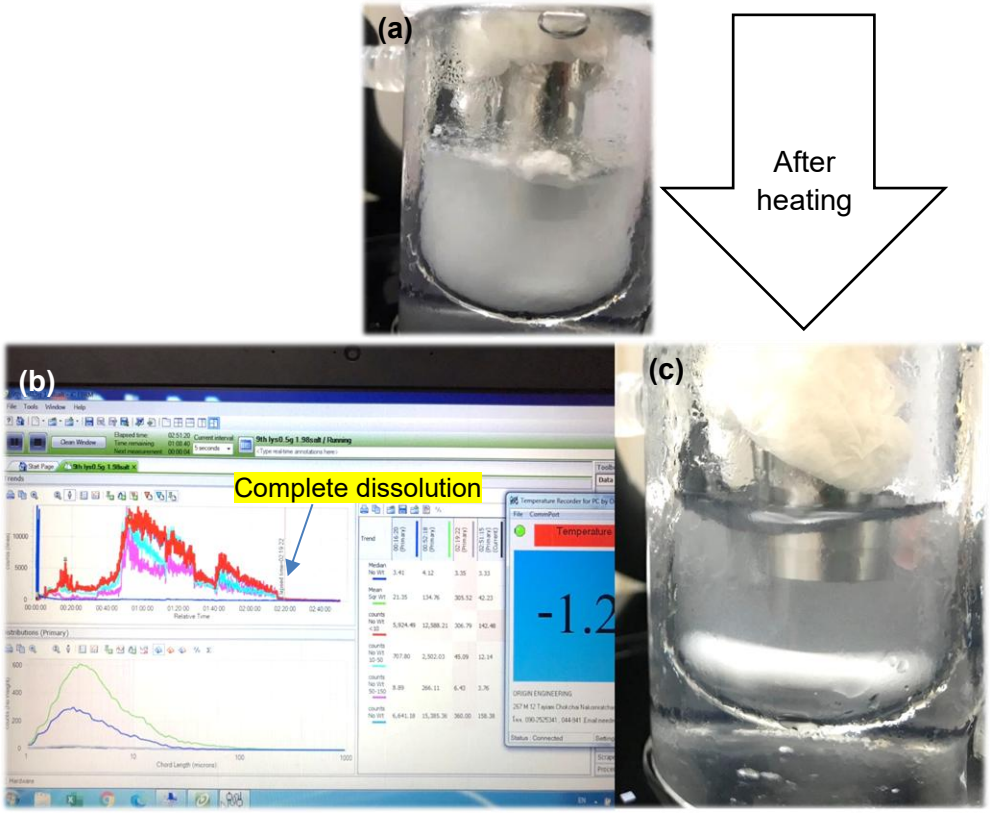

Figure 4.1: The crystallizer with FBRM set-up for measuring lysozyme solubility.

The solubility of lysozyme in different amount of ammonium sulfate is shown in Figure 4.2. The solubility of lysozyme decreased with increasing the concentration of ammonium sulfate and increased with raising temperature (Do et al., 2021; Ferreira & Castro, 2023). The phase-diagram to control SFO process for lysozyme that completed all three different salt concentration are shown in Figure 4.3. The result illustrated freezing the water out and nucleation of lysozyme were reached higher solubility point. Nucleation points at 0.7 M of salt was less than using 0.4 M and 0.6 M. It followed the literature (Elizabeth L. Forsythe, Edward H. Snell, Christine C. Malone, & Pusey, 1999) and solubility of 0.4 and 0.6 M illustrated the over salt drove the less dissolution ability, but the 0.7 M condition uncapable produced crystalline of lysozyme as shown in Figure 4.4 (c).

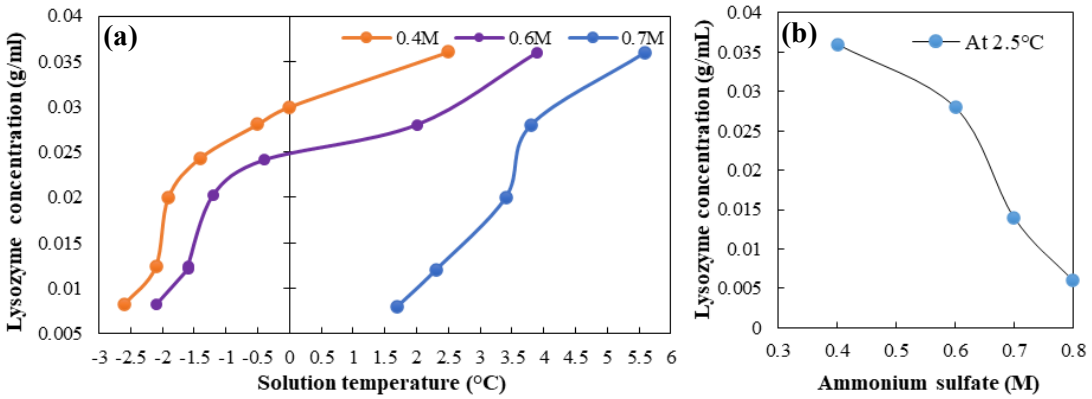

Figure 4.2: Solubility of lysozyme in ammonium sulfate with various temperatures (a-b).

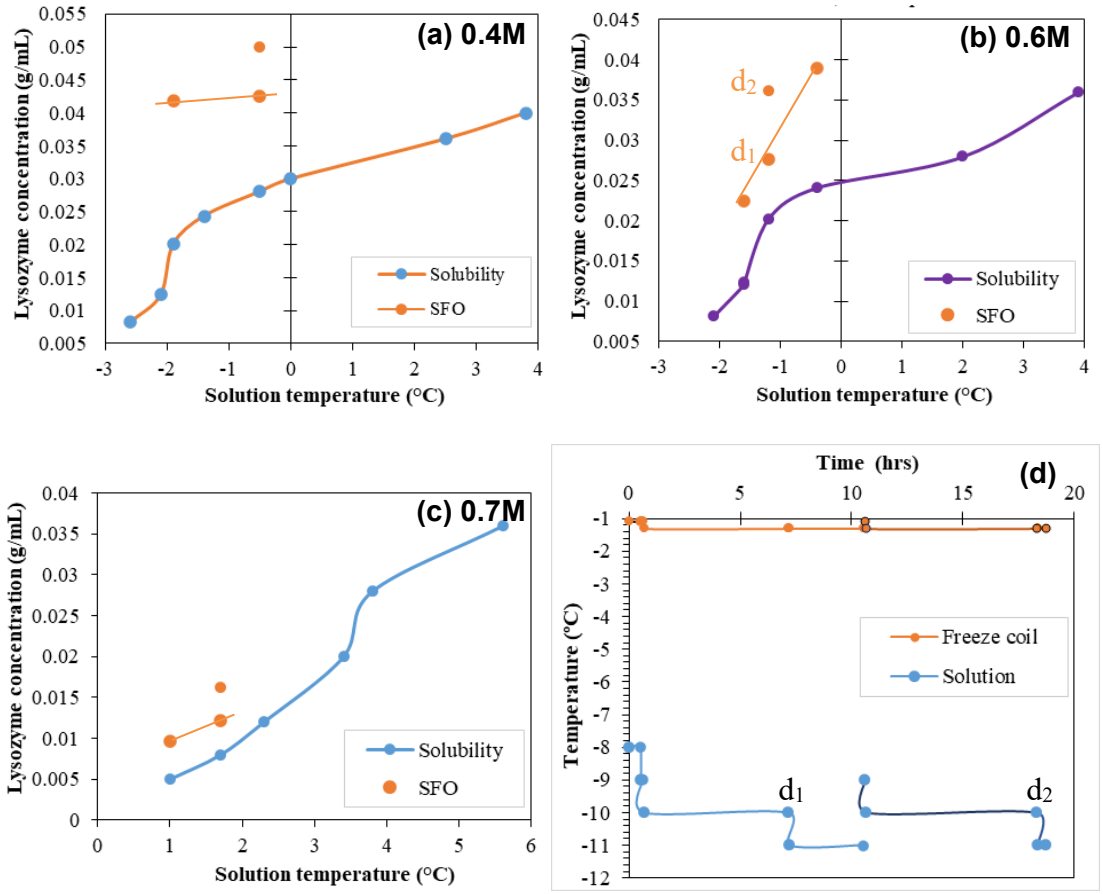

Figure 4.3: The phase-diagrams of lysozyme in ammonium sulfate solution. Solubility and nucleation point using SFO at pH 4.6 with salt concentration of (a) 0.4M, (b) 0.6M, and (c) 0.7M. (d) Freeze-coil and bulk-solution temperature profiles with time.

In Figure 4.4, showed the lysozyme became cloud (nucleation) in SFO crystallizer. Figure 4.4 (a) was before and after freezing the water until clouding of salt 0.7M at 1 ˚C. The observed particle image under microscope in Figure 4.4 (b) and the filtration and dryness in (c). But after filtration the cloud solution became gel-like because over salt addition. After drying, the salt crystal nucleated over the lysozyme.

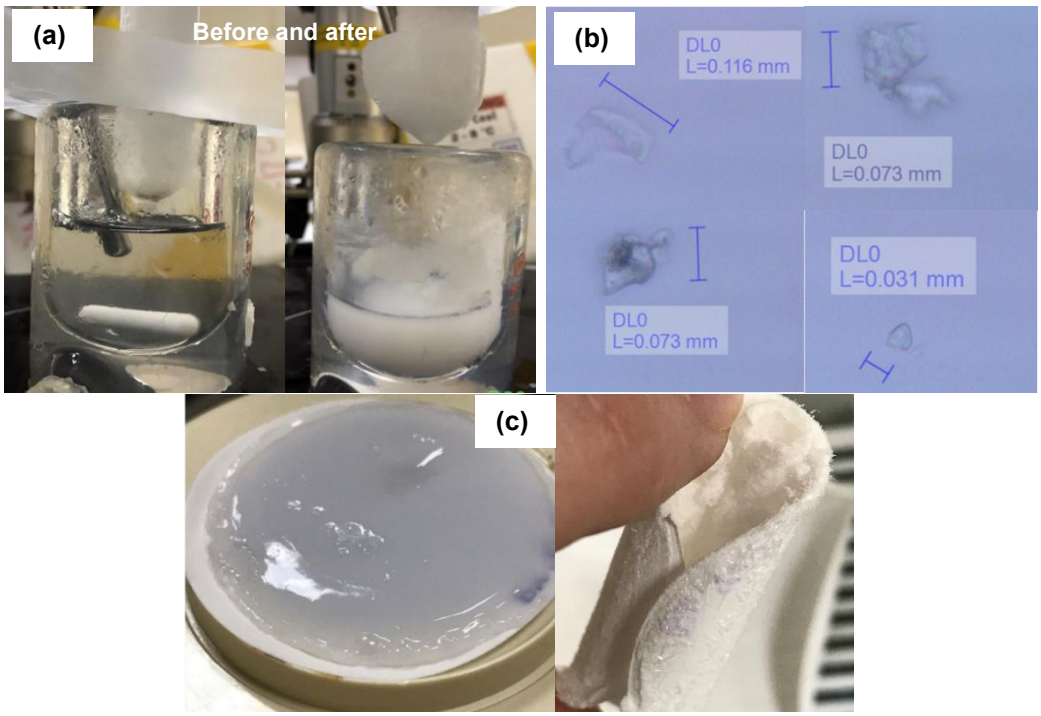

Figure 4.4: (a) The SFO crystallizer at Lysozyme precipitated as a gel in ammonium sulfate (0.7M) from solution at 1 °C. (b) particle images by Microscope,4X. (c) Filtration and dry particle.

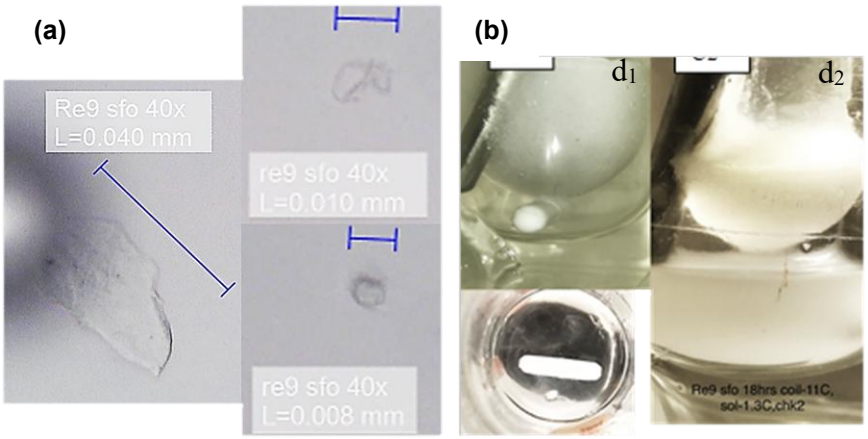

Figure 4.5: The Lysozyme nucleation in ammonium sulfate (0.6M) from SFO crystallization: (a) particle images by Microscope 40X, and (b) Lysozyme cloud in solution but d_1 as a first freezing, d_2 as second freezing.

For 0.6M of salt, the freezing water out required to run for second time due to less cloud occurred at first freezing (Figure 4.5 (b), at points d_1 & d_2). However,

the all particle image showed unlike lysozyme particle when compared to previous work (crystallization of chicken egg white lysozyme from assorted sulfate salts) (Elizabeth L. Forsythe et al., 1999). The final temperature could be controlled to only −11 ˚C for this concentration and by freeze rate of 0.1 ˚C/min for freeze coil. The chosen freezing rate may have been too high, promoting gelation and poor crystal habit; provide comparative runs at slower rates to corroborate.

To summary, solubility of lysozyme decreased with increasing ammonium sulfate concentration. Ammonium sulfate contributed lysozyme cloud in SFO crystallizer, but crystal was still small and disable to observe the monoclinic form by microscope while comparing to case of NaCl. For this study, SFO technique had satisfy efficiently to drive solution to supersaturation and it must be studied more to use in other protein separation/crystallization. However, this need to be careful the final temperature of freeze coil, initial enzyme concentration, and amount of salt or precipitant agent to avoid precipitation and loss of enzyme.

4.2 Results of papain crystallization

4.2.1 Solubility of papain

Solubility studies revealed that papain exhibited similar saturation concentrations in both DI water (pH 6.6-7) and acetate buffer (pH 5.0), as evidenced by the overlapping solubility curves shown in Figure 4.6 (a). This observation suggests that the buffer system at pH 5.0 did not significantly alter the thermodynamic solubility of papain compared to aqueous solution (pH 6.6). Opposite with lysozyme that solubility was increased by raising pH (Wang et al., 2023). But this point suitably studies more. Figure 4.6 (b) presents the solubility profile of papain in methanol-acetate buffer mixtures, showing a clear dependence on both solvent composition and temperature. The solubility decreases progressively with increasing methanol fraction (w/w), following typical antisolvent behavior where the addition of methanol reduces the solubility of papain. Similar solubility suppression has been reported for lysozyme, amino acids and peptides exposed to alcohol–acetate environments, attributed to decreased dielectric constant and disrupted hydrogen bonding networks that promote aggregation (Do et al., 2021; Ferreira & Castro, 2023).

Furthermore, lower temperatures resulted in lower solubility at all methanol fractions, consistent with the exothermic nature of protein dissolution and corroborated by thermodynamic analyses of acetate-buffered protein systems (Grossmann & McClements, 2023; Hentschel et al., 2021; Kenneth P. Murphy, Privalov, & Gill, 1990).

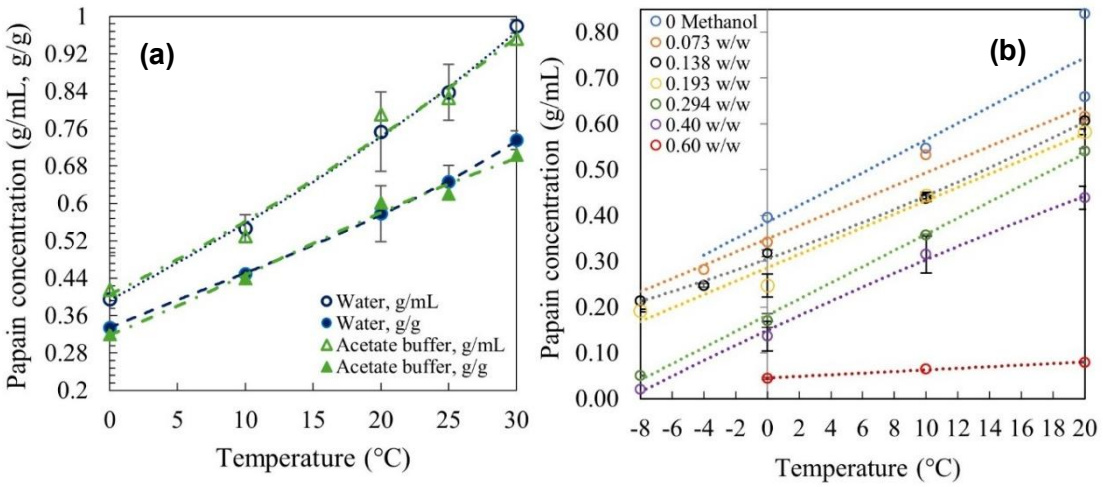

Figure 4.6: The solubility of papain in (a) water and acetate buffer (pH 5.0) at various temperatures. (b) In the mixture of acetate buffer with methanol (0.07-0.6 w/w) at various temperatures.

4.2.2 Cooling crystallization for papain

The cooling crystallization experiments revealed distinct nucleation characteristics under different conditions. When a saturated papain solution (0.97 g/mL) at 30 °C was cooled at rate of 0.005 °C/min with moderate agitation, the cloud point (indicating nucleation onset) was observed at 12.5 °C. The gradual viscosity increased at lower temperatures reduced stirring efficiency, as evidenced by the slower rotation of the magnetic stir bar. In contrast, under static conditions, nucleation was delayed until 9.0 °C, demonstrating the significant impact of agitation on crystallization kinetics (Bartłomiej Filip, Michał Kołodziej, Roman Bochenek, Marcin Chutkowski, & Antos, 2024; Noor et al., 2020). For solutions with lower initial saturation (0.7534 g/mL at 20 °C), nucleation occurred at −3.0 °C, although some batch-to-batch variability was observed. The induction time of cooling crystallization for papain from saturation (at 30 to 9 °C) was evaluated approximately 15 hours for nucleation and growth in case

of smoothly agitation, but in case of none agitation because of high viscosity that induction time was approximately 55 hours (showed in appendix A.1). The complete phase behavior, including the boundaries of the supersaturation zone, is presented in Figure 4.7.

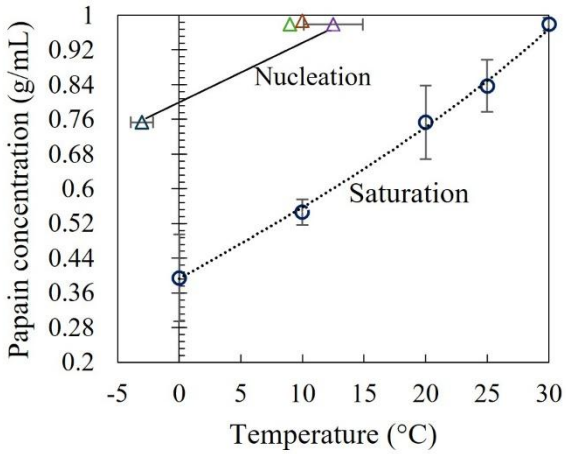

Figure 4.7: The phase-diagram for cooling crystallization of papain.

Crystallization and photomicroscopes analyses (Figures 4.8 and 4.9) suggest that crystal habits are likely dependent on the initial concentration and temperature. The −3 ℃ system produced metastable needle-like crystals that exhibited partial redissolution, while the 12.5 ℃ system initially formed sharper needle crystals, which transformed into plate-like or mixed morphologies during extended growth. These observations align with previous reports of papain's needle-like crystalline structure at nucleation point (Harris, 1983). The large temperature difference between the −3 ℃ system and the ambient environment may explain the observed redissolution under the microscope. However, the plate-like habit of papain crystal has not been reported previously. So, the plate-like habit of papain crystal needs more research for fulfilling the confirmation.

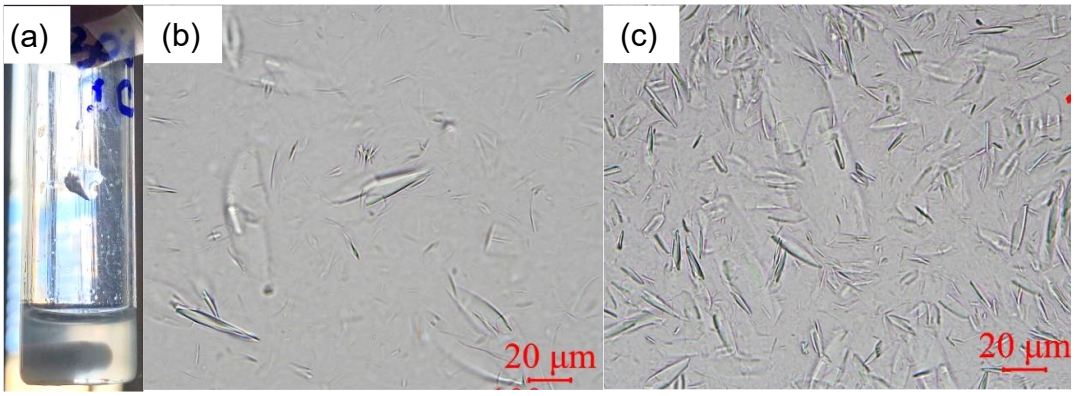

Figure 4.8: Cooling crystallization (cooling from 30 °C to 12.5 °C) of a saturated papain solution: (a) solution clouding in the crystallizer, (b) photomicrograph of crystals at the onset of nucleation, and (c) photomicrograph of crystals after 24 hrs of nucleation and growth.

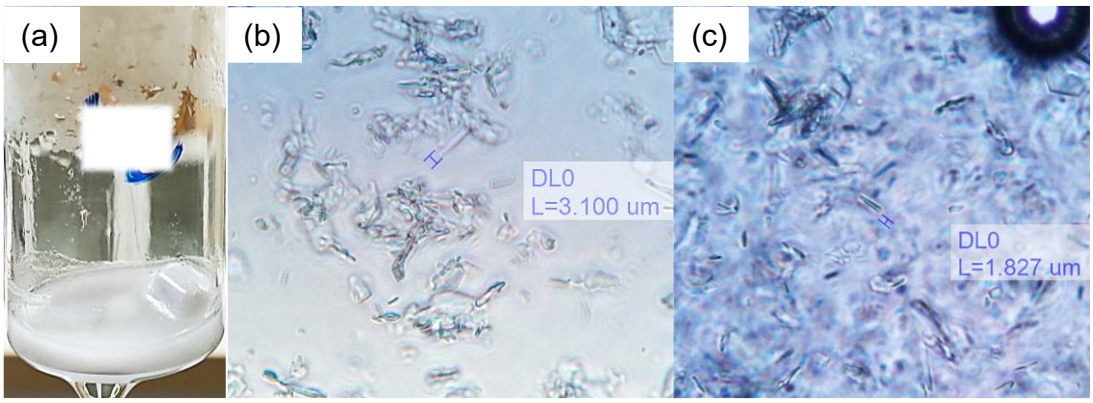

Figure 4.9: Cooling crystallization (cooling from 20 °C to -3 °C) of a saturated papain solution: (a) crystal clouding in the crystallizer after nucleation, (b) photomicrograph of crystals at the onset of nucleation, and (c) photomicrograph of crystals after 24 hrs of nucleation and growth.

4.2.3 Antisolvent crystallization for papain

Phases diagram of antisolvent crystallization for papain using methanol is illustration in Figure 4.10. The antisolvent crystallization of papain was systematically investigated at two fixed temperatures (20 °C and 0 °C) by incrementally adding methanol (0.2 mL/20 min) into saturated solutions until nucleation occurred. At 20 °C, a solution with an initial concentration of 0.67 g/mL reached its cloud point at a methanol weight fraction of 0.231, while a more dilute solution (0.07 g/mL) required significantly more antisolvent (methanol fraction of 0.66) to induce nucleation (Figure

4.10 (b)). In contrast, at 0 °C, nucleation occurred at lower methanol fractions for concentrated solutions (0.4 g/mL at methanol weight fraction of 0.112), but required higher fractions for dilute systems (0.1 g/mL at methanol weight fraction of 0.514) (Figure 4.10 (a)). The different methanol requirements at each temperature (0.231 w/w at 20 °C vs 0.112 w/w at 0 °C for concentrated solutions) demonstrate that temperature significantly affects the antisolvent concentration needed for nucleation. This suggests that methanol's disruption of papain's solvation shell prevents ordered crystallization regardless of temperature (Chayen & Saridakis, 2008; Mullin, 2001).

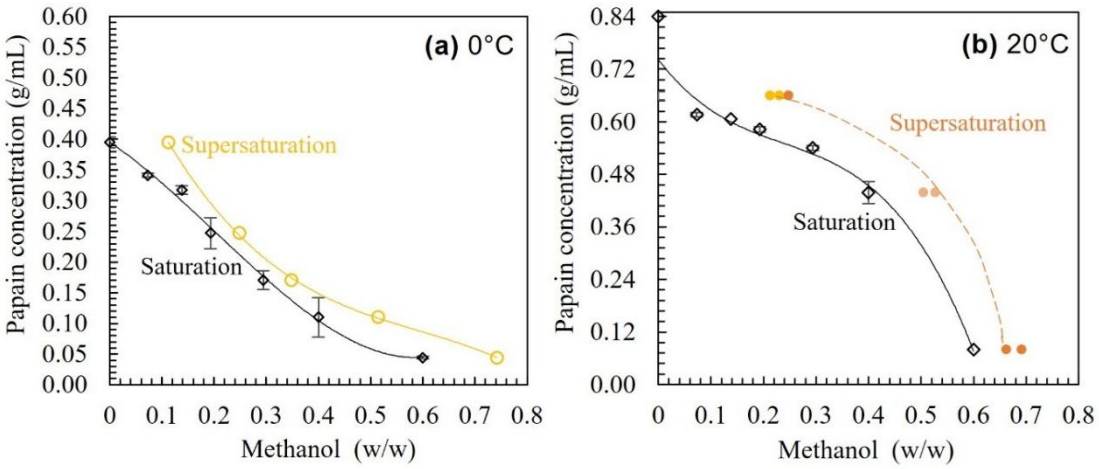

Figure 4.10: The phase diagram of antisolvent crystallization for papain at 0 °C (a) and 20 °C (b).

The real-time monitoring by FBRM and Easy-viewer (PVM) revealed (Figure 4.11) that particle formation began immediately after reaching the cloud point, with turbidity increasing as methanol was added.

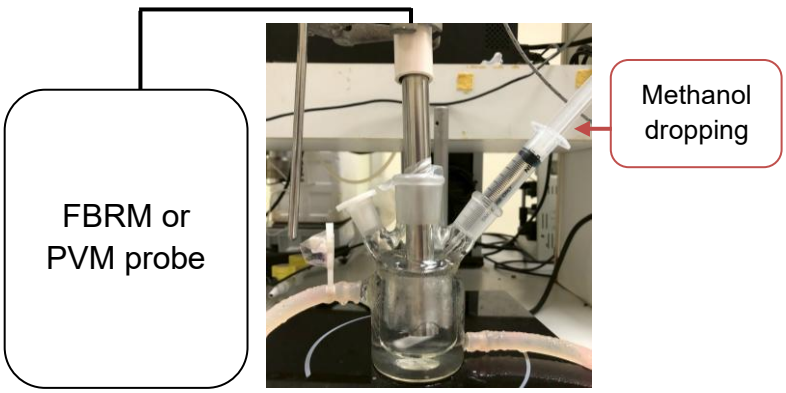

Figure 4.11: Antisolvent crystallizer setup with methanol dropping.

As shown in the photographs of Figure 4.12, the 0.17 g/mL solution at 0 °C showed initial nucleation at methanol fraction of 0.31-0.348 w/w, followed by rapid particle growth beyond 0.52-0.56 w/w, eventually forming a gel above 0.57 w/w. In Figure 4.13, the photographs of crystallizer show the solution at supersaturation level upon methanol addition at 0.21-0.23 w/w from a 0.67 g/mL solution at 20 °C (Figure 4.13 (a)). Gelation started occurred at 0.64 w/w of addition methanol (Figure 4.13 (c)). However, all conditions ultimately produced amorphous precipitates rather than crystals, consistent with previous reports using ethanol (Boonkerd & Wantha, 2024). Even though, harvesting the particle from cloud points using centrifugal force and gravity separation, the particle became amorphous as evidenced by the PXRD pattern shown in Figure 4.17.

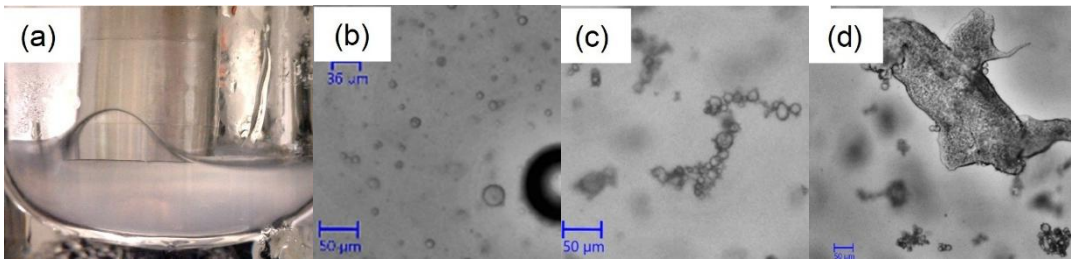

Figure 4.12: (a) Crystallizer image was captured during methanol addition at 0.348 w/w, and photomicrograph of papain crystals in liquor (b) at cloudy point (methanol 0.348 w/w) from saturation concentration of 0.17 g/mL (0 °C); (c) at point of methanol 0.56 w/w, and (d) the particle became sticky gel at 0.57 w/w.

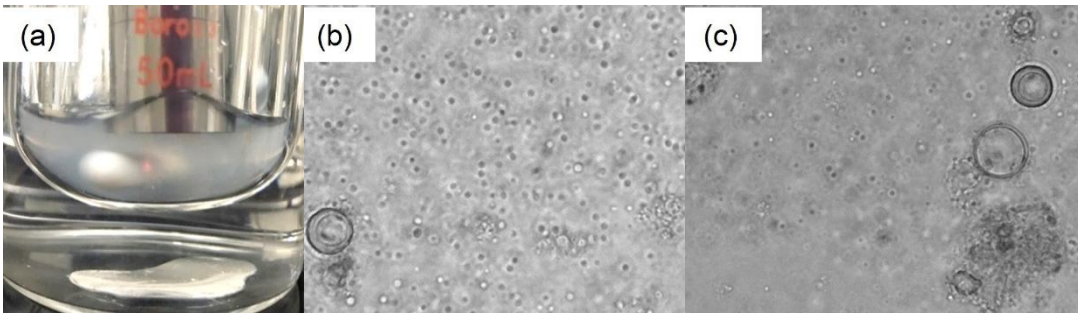

Figure 4.13: (a) Crystallizer captures image was captured during methanol addition at supersaturation of 0.23 w/w, and photomicrograph of papain crystals in liquor (b) at cloudy point (0.23 w/w) from saturation concentration of 0.67 g/mL (20 °C) and (c) the particle became sticky gel at 0.64 w/w.

4.2.4 SFO crystallization for papain

Solvent freeze-out crystallization was systematically investigated at three initial concentrations 0.47 g/mL, 0.41 g/mL, and 0.33 g/mL; to observe the nucleation points at different temperatures range from −1.5 to 1 °C. The phase diagram for this SFO process of papain is shown in Figure 4.14 (a). The system achieved remarkably high nucleation thresholds, indicating the significant supersaturation required to initiate crystal formation. Crystalline was monitored via optical microscopy (40x magnification) following nucleation after deactivation of the freezing coil.

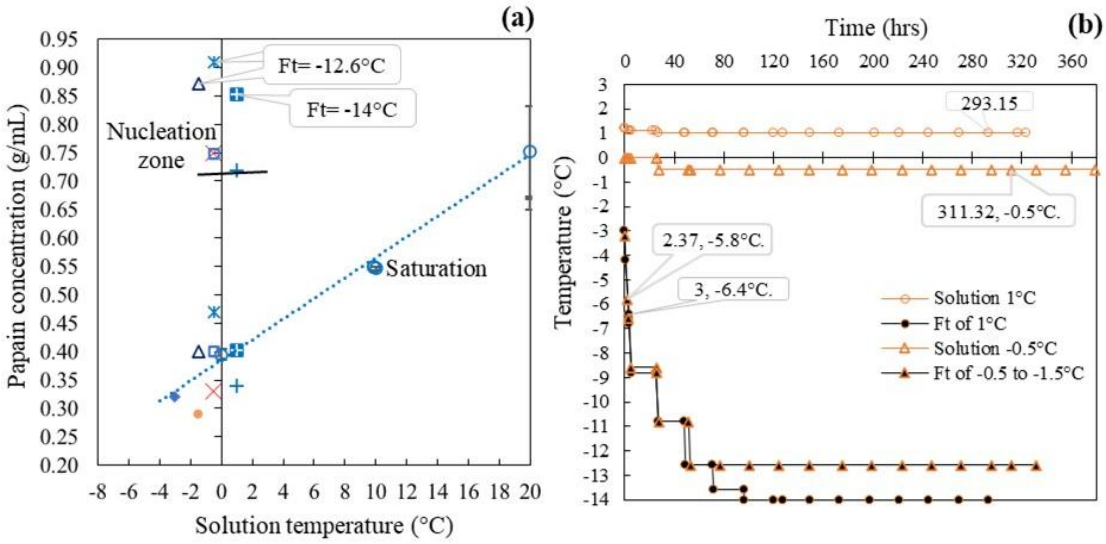

Figure 4.14: (a) The phase diagram of SFO for this papain solution at pH 5.0. (b) the temperature reduction profile of freeze coil (293.15 & 311.32h are time of nucleation). **Ft is final temperature of freeze coil*.

The final temperature of freeze coil terminated at -14 °C for systems maintained at 1 °C of papain solution as shown in Figure 4.14 (b). This is compared to −12.6 °C for both −0.5 °C and −1.5 °C of papain solution. The SFO process at low temperature (close to 0 °C) induced cloud concentration at-least 0.7157 g/mL (feed 0.33 g/mL saturation of 1 °C) in a residual volume 3.15 mL, corresponding to an 18.51% recovery with 13.22% lost in ice, as detailed in Table 4.1. Comparative analysis revealed that reduced final volumes (residual 1.9 mL, 0.7482 g/mL from feed 0.33 g/mL at −0.5 °C) recovered higher percentages (20%), demonstrating the expected concentration-dependent efficiency. Micrographic examination (Figures 4.15)

consistently revealed needle-like crystal morphologies under all experimental conditions, which transformed into a mixed of plate-like after drying as shown in Figure 4.16. The secondary nucleation may be occurred during slowly drying.

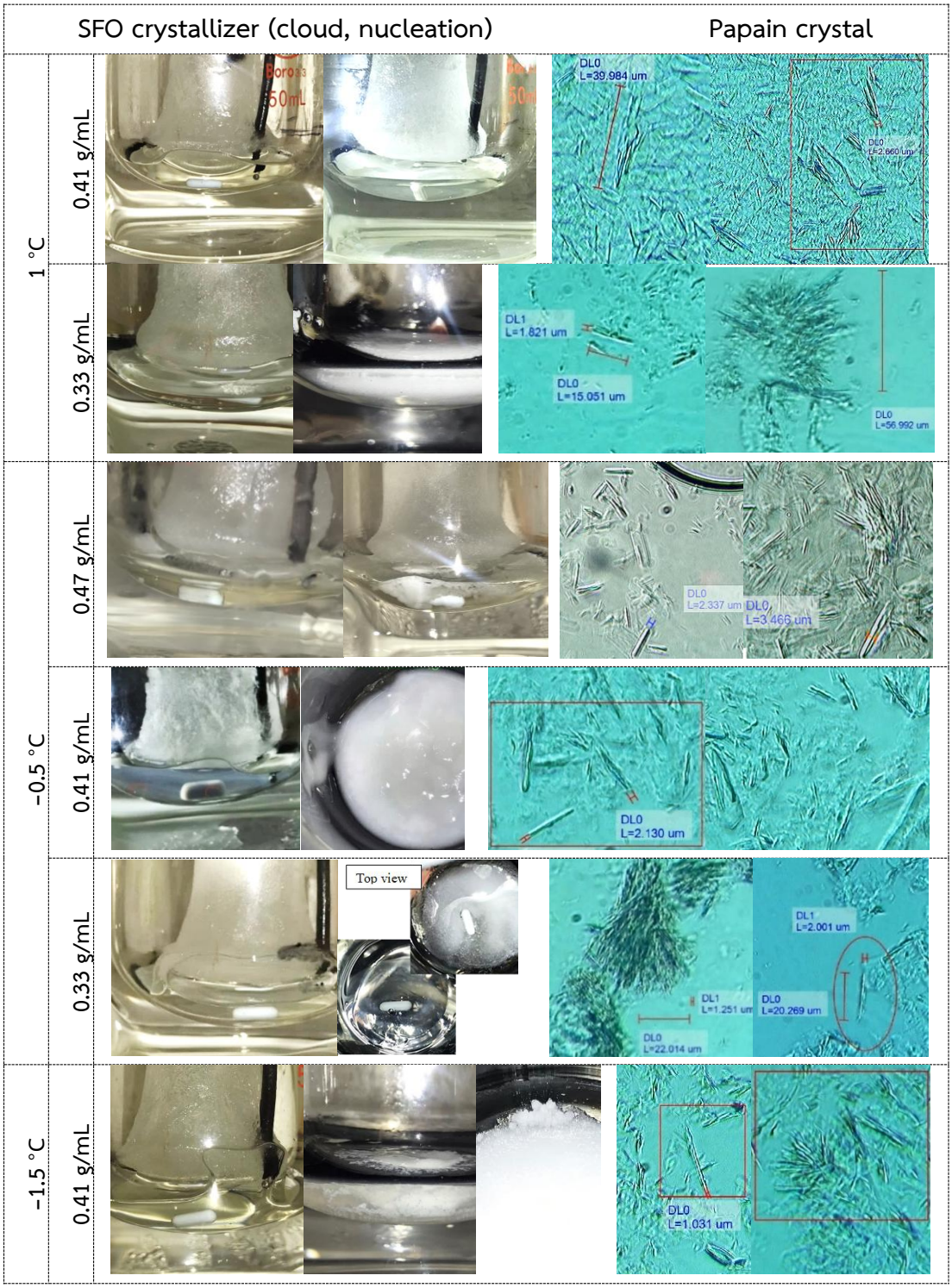

Figure 4.15: The SFO crystallizer and photomicrographs of papain crystal obtained at nucleation point from feed concentrations ranging of 0.33 to 0.47 g/mL.

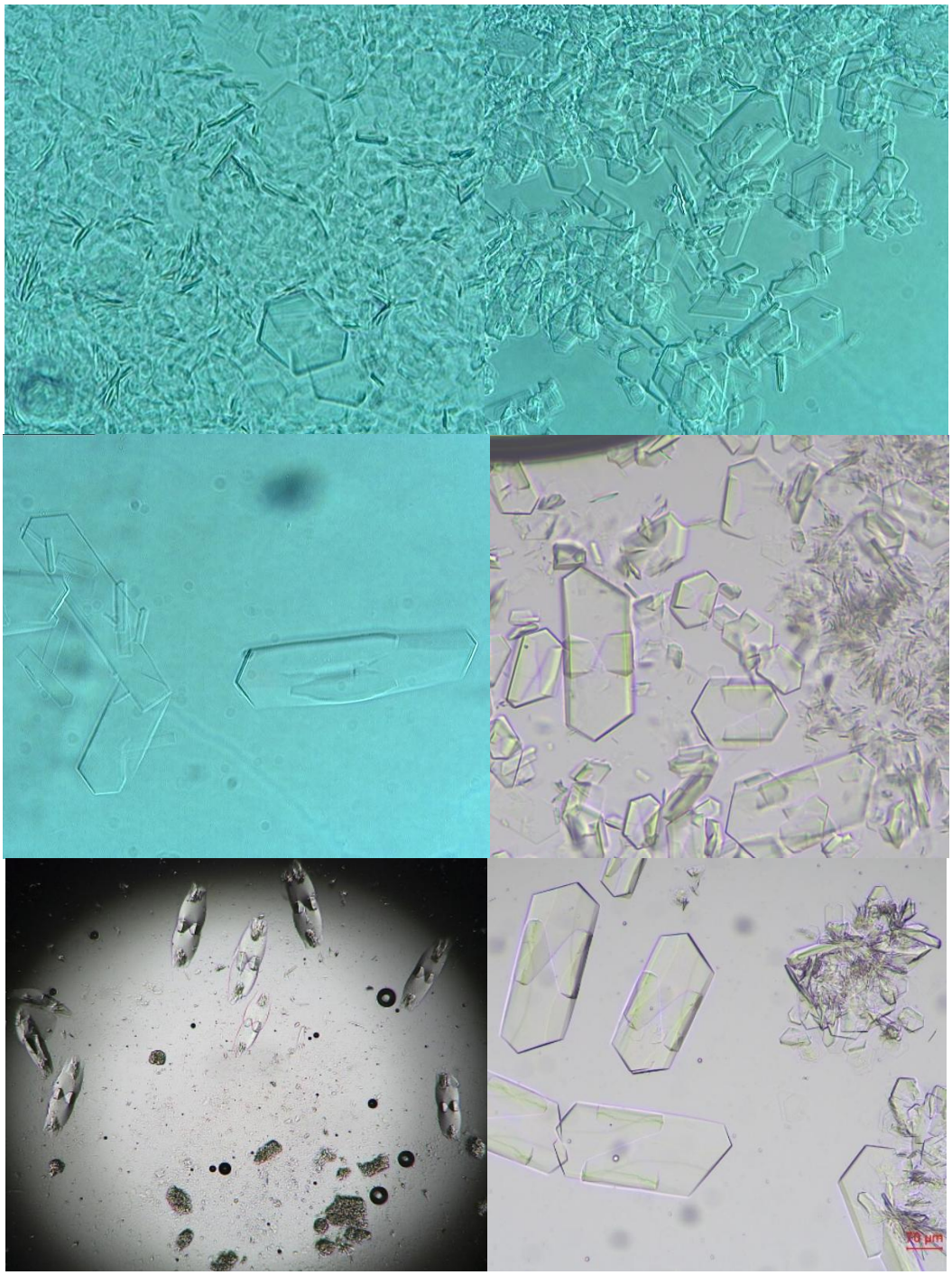

Figure 4.16: Examples of photographs of crystals from all conditions obtained after drying on slide under microscope (room/air temperature) in SUT and TjU.

Table 4.1: The percentage loss and recovery of papain crystallization using SFO in this work.

Papain in acetate buffer (no methanol addition)						
Solution Temp,°C	Initial Solution concentration, g/mL	Concentration at cloud points, g/mL	Residual Volume, mL	Ice Volume, mL	%Recovery of papain	%Lost of papain in ice
1	0.41	0.8472	1.8	5.2	64.74	28.89
−0.5	0.47	0.9222	2.6	4	64.21	21.23
	0.41	0.7449	2	5	57.14	26.02
	0.33	0.7482	1.9	5.1	20.05	20.58
−1.5	0.41	0.8671	1.2	5.75	58.42	26.77

The SFO technique demonstrated particular effectiveness for near saturated concentration systems, achieving recoveries exceeding 55% at all tested temperatures (−1.5, −0.5, and 1 °C) while minimizing solute loss to ice entrapment. Although the process required extended duration to reach nucleation, the reproducible formation of crystalline products (in contrast to the amorphous aggregates observed in antisolvent crystallization) highlights the method's superiority for obtaining structurally defined papain crystals.

This systematic investigation demonstrates that solvent freeze-out (SFO) crystallization enables precise, temperature-programmed control of nucleation while preserving protein tertiary structure and enzymatic activity (Ming et al., 2021), were mention in section 4.2.7. In contrast to traditional salting-out methods that risk structural denaturation at high ionic strengths (Hekmat, 2015; Wang et al., 2023), SFO produces homogeneous, needle-like crystals with sharply defined, temperature-dependent nucleation and growth thresholds (Feng et al., 2024; McArdle & Erxleben, 2024). These thresholds align with lysozyme pseudo-phase boundaries reported by Díaz-Borbón et al., (Borbón & Ulrich, 2012; Borbon & Ulrich, 2013) validating cross-system reproducibility. The observed habit modulation via additive concentration and cooling rate mirrors needle-forming strategies in organic crystallization systems, highlighting SFO's advantage for morphology control in biopharmaceutical scale-up (Xiaoxi Yu et al., 2015).

4.2.5 Powder X-ray diffraction

This work was further examined using PXRD, as shown in Figure 4.17. The papain crystal exhibited the characteristic peaks at 2theta angle of 12.13°, 14.83°, 18.97°, 20.19–20.80°, 23.34°, 28.65° and 36.00°, consistent with patterns of the commercial papain and previous reports (Chandran & Nachimuthu, 2018; Qi Hao et al., 2024). The products obtained from the SFO process and cooling process (pH 5 and 6.7) showed similarly high crystallinity and phase purity, whereas the antisolvent-derived product was amorphous (Boonkerd et al., 2024) due to XRD pattern showed as curve (no peaks).

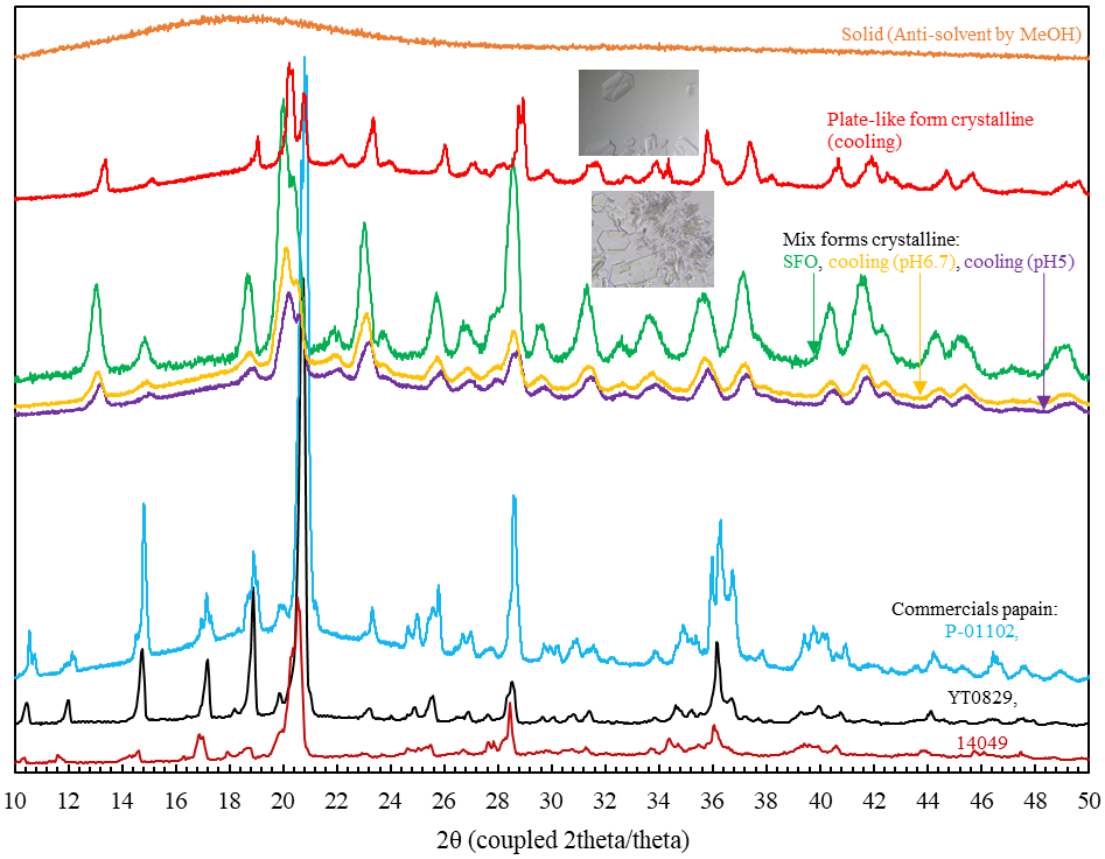

Figure 4.17: PXRD patterns of papain particle obtained from this work: orange) Amorphous papain from antisolvent by methanol; red) Plate-like form from cooling crystallization; green) Mixed needle/plate like habit crystal of papain from SFO process; yellow) Mix form crystal from cooling crystallization without buffer; purple) Mix form crystal from cooling crystallization with buffer (pH 5.0); and commercial crystalline papain: blue) As product no. P-01102; black) YT0829; dark red) 14049.

4.2.6 SEM of papain crystal

The SEM photographs in Figure 4.18 further revealed distinct morphologies. Commercial papain (Figure 4.18 (a)) appears as irregular, smooth-surfaced granules, while SFO-derived papain crystals (Figure 4.18 (b-e)) exhibits two habits: agglomerated plate-like lamellae in panel (c) and agglomerated needle-like crystals in panel (d-e). The crystals in (b-e) contrasted with the SEM observations of antisolvent-precipitated papain which formed agglomerated granule (Boonkerd et al., 2024). The high viscosity of the remaining solvent and slow drying process (in air/room environment) likely drove the agglomeration of the papain crystal (Gao et al., 2024; Qi Hao et al., 2024).

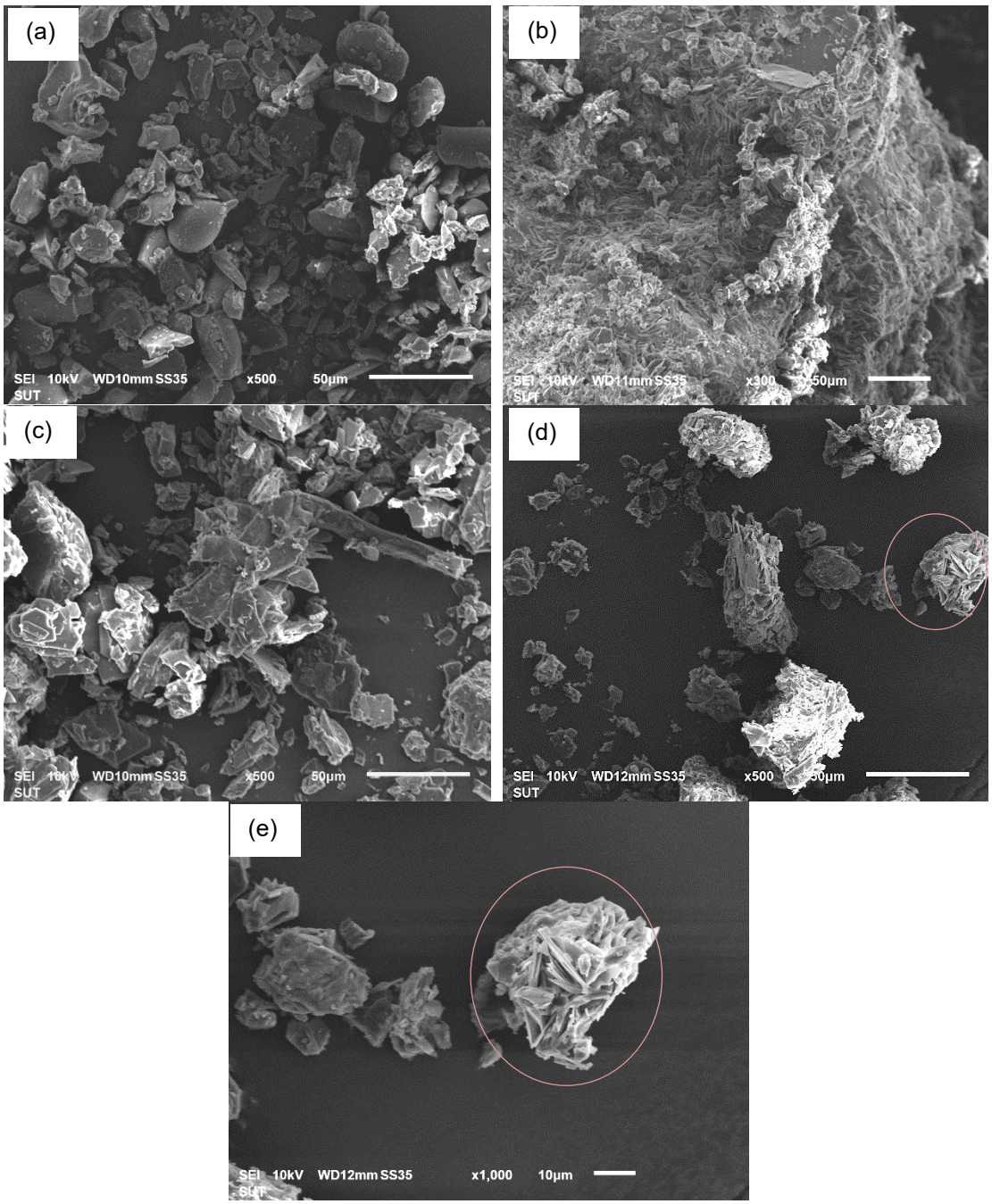

Figure 4.18: The SEM photographic of this work: (a) Commercial crystalline papain, (b-e) Crystal of papain from SFO process. (c) Plate-like form and (d-e) Needle-like form.

4.2.7 The enzyme activity analysis

Papain crystals obtained from the SFO crystallization and commercial papain were each tested at a concentration of 30 mg/mL for their reaction with the substrate, and the resulting product was measured at 410 nm, as shown in Figure 4.19.

The enzyme activity was then calculated, and the specific activity is shown in Table 4.2. The results showed the papain crystal obtained activity from SFO crystallization was 0.001777 BAPNA Units, while commercial papain crystal responded an activity of 0.001811 BAPNA Units. At the same time, papain crystal from the antisolvent crystallization responded the stable enzyme activity. It may cause of antisolvent method consumes shorter processing time (not over 20hrs), but SFO and cooling process maintained longer processing time (over 50 hours) for papain in liquid-phase before the occurrence of nucleation. As consistence with illustration in Figure 4.20 all showed that the papain from liquid-phase storage reduced enzyme activity faster than keeping as solid-phase (crystal) under cool environment during a month. The crystal from SFO (0.0000590 Units/mg) and cooling (0.0000596 Units/mg) were between the commercial papain (0.000060 Units/mg) and liquid-phase storage of papain (0.0000570 Units/mg). These values indicate that the enzymatic function was preserved, consistent with previous studies showing that antisolvent crystallization (particularly using ethanol or methanol) can maintain protease activity when solvent ratios and temperature are controlled (Boonkerd & Wantha, 2024; Sirirak et al., 2025).

The negligible difference in activity between papain crystals obtained from SFO and commercial papain supports the hypothesis that solvent freeze-out crystallization is a gentle, non-denaturing technique suitable for biopharmaceutical applications. Similar findings were reported by Arnon (Ruth, 1970) and Boonkerd (Boonkerd et al., 2024) who demonstrated that papain retains catalytic efficiency post-crystallization when stabilized with cysteine and EDTA, and assayed using BAPNA substrates. These results further reinforce the suitability of crystallization for preserving bioactivity in proteolytic enzymes.

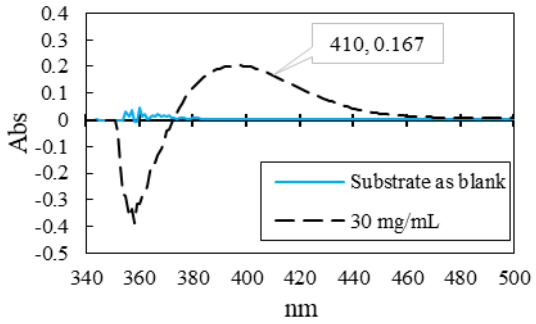

Figure 4.19: The product from reaction of papain with substrate (BAPNA) was analyzed using UV-vis spectroscopy at 410 nm.

Table 4.2: The enzyme activity assay of papain crystal.

Source of papain crystal	BAPNA Units	Units/mg
Commercial (YT0829)	0.001811	0.000060
By cooling crystallization	0.001788	0.0000596
By anti-solvent crystallization using methanol	0.001883	0.000063
By SFO crystallization	0.001777	0.000059

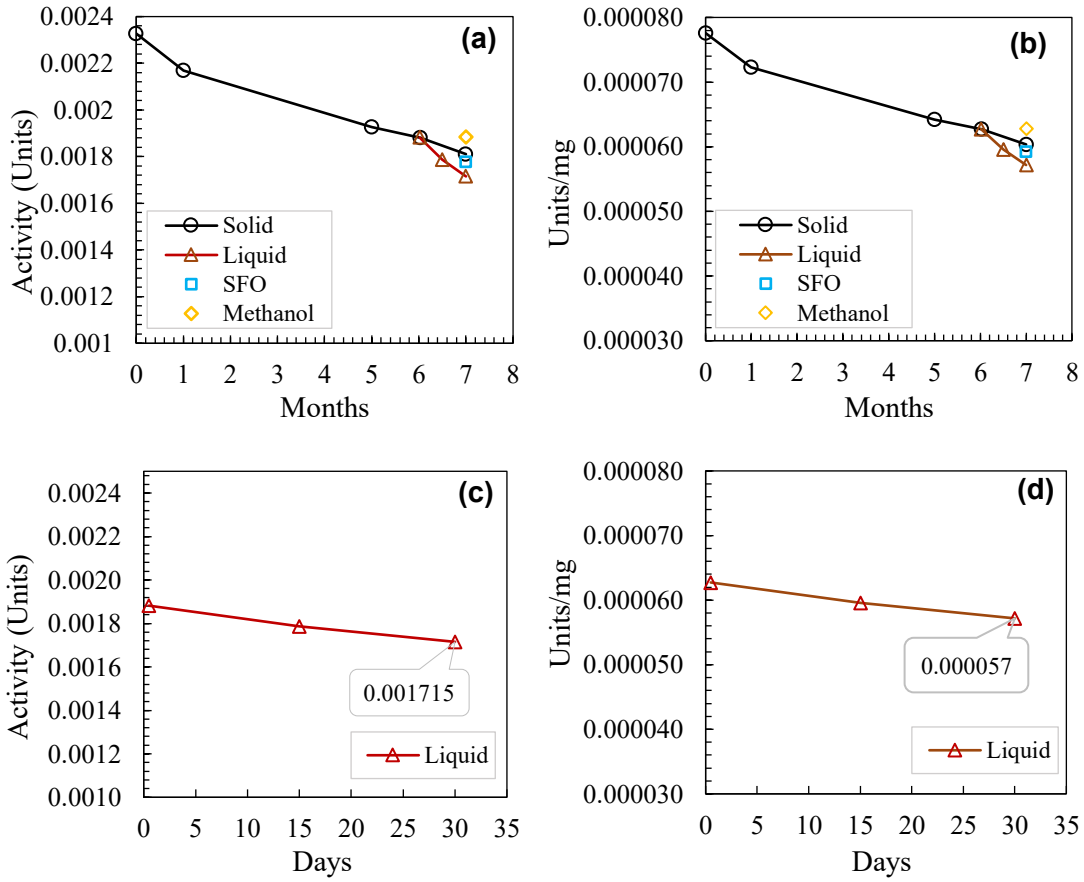

Figure 4.20: The papain activity denatured by time in different phases storage inside refrigerator (solid commercial papain and dissolution in water as liquid) and comparison with products of using antisolvent by methanol, SFO process: (a) as BAPNA Units, (b) as Units/mg. The activity denatured in liquid phase: (c) as BAPNA Units, (d) as Units/mg.